

Stabilization of rock salt ZnO nanocrystals by low-energy surfaces and Mg additions, a first principles study: Supporting Information

R.S. Koster,* C.M. Fang, M. Dijkstra, A. van Blaaderen, and M.A. van Huis*

*Soft Condensed Matter, Debye Institute for Nanomaterials Science, Utrecht University,
Princetonplein 5, 3584 CC Utrecht, The Netherlands*

E-mail: r.s.koster@uu.nl; m.a.vanhuis@uu.nl

Introduction

This Supporting Information contains:

- A discussion of the dilute case,
- Figure regarding the lattice parameters as a function of x ,
- Figures of the slabs used in the surface energy calculations,
- Details regarding the Hubbard U parameter,
- Figures of the Bader charge distribution in the slabs,
- A description of the functions used to determine the phase diagram (Fig. 10).

*To whom correspondence should be addressed

For the DFT calculations, the first principles Vienna Ab-Initio Simulation Package¹ (VASP) code was used. For a description of DFT in general, we refer to the original papers of Kohn and Sham.²⁻⁴ The Generalized Gradient Approximation functional by Perdew, Burke and Ernzerhof^{5,6} (GGA-PBE) was used within the projected augmented wave (PAW) method.⁷ A cut-off energy of 600 eV was used for the wavefunctions, and a cut-off of 900 eV for the augmentation charges. A Hubbard U correction of was used to better describe Zn $3d$ electrons.

The dilute case

To asses the reliability of our calculation, we first consider the dilute case of ZnO-MgO mixing. A dilute amount of Mg in ZnO does not produce large differences in the WZ structure. Upon replacing one of the 54 Zn atoms in the WZ ZnO supercell with Mg, the lattice parameter a increases only slightly, 0.027%, while the c lattice parameter decreases by 0.02%. Changes in the positions of the atoms are minimal as well: displacements of the nearest O and Zn atoms are only 0.006 Å. A similar effect can be seen for a Zn atom in RS MgO. The lattice parameters a and c increase 0.007% and 0.016% respectively. The nearest O atoms relax 0.018 Å away from the Zn atom, while the nearest Mg atoms relax 0.004 Å towards the Zn atom.

In Fig. S1 the densities of states are shown for pure ZnO and for ZnO with a single Mg defect. The density of states for ZnO does not seem to be affected much by the single Mg atom. In fact, the Mg atom donates most of its electrons to the O states, such that the projected density of states of the Mg atom is so small that it can not be seen in the Fig. S1. The difference between pure MgO and MgO with a single Zn defect (Fig. S2) is clearer, since the Zn $3d$ states are prominently visible, but also in this case the effects on the band gap appear negligible.

To estimate the effects of the ordering of the atoms in the supercells, ΔE was determined for ZnO supercells, where two Zn atoms were replaced with Mg atoms, both for the case

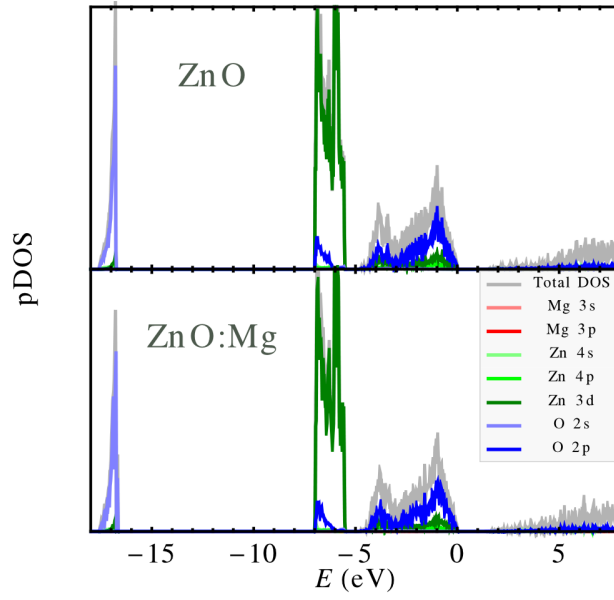


Figure S1: Projected DOS plots for pure ZnO (Top), ZnO with one Mg defect (Bottom).

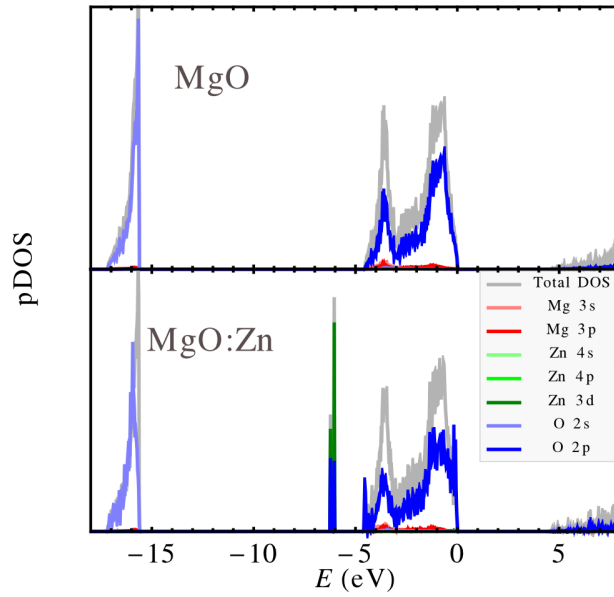


Figure S2: Projected DOS plots for pure MgO (Top) and MgO with a Zn defect (Bottom).

where the distance between the Mg atoms was minimal and the case where it was maximal. The results shown in Table S1 indicate that differences are less than 1 meV per formula unit, which is not significant. From this we conclude that the energy for a particular configuration will likely be representative for all configurations with the same value of x .

Table S1: A comparison of formation energies of nearby and distant Mg atoms in ZnO supercell (i.e. $x = 2/54$, 2 Mg atoms, 52 Zn atoms and 54 O atoms), and vice versa.

		ΔE_{far} (meV)	ΔE_{close} (meV)	$\Delta\Delta E$ (meV)
RS	$\text{Mg}_2\text{Zn}_{52}\text{O}_{54}$	268.3	268.2	0.1
RS	$\text{Mg}_{52}\text{Zn}_2\text{O}_{54}$	8.7	8.3	0.2
WZ	$\text{Mg}_2\text{Zn}_{52}\text{O}_{54}$	4.0	3.8	0.2
WZ	$\text{Mg}_{52}\text{Zn}_2\text{O}_{54}$	129.9	129.5	0.4

Lattice constants as a function of x

In our calculations, hexagonal supercells were used, for all three crystal structures RS, WZ, and ZB. For RS and ZB, the hexagonal lattice parameters are related to the cubic lattice parameters via $a_{\text{hex}} = \frac{a_{\text{cub}}}{\sqrt{2}}$ and (ideally) $c_{\text{hex}} = \sqrt{3}a_{\text{cub}}$. In Figure S3 the lattice parameters a, c and their ratio c/a of $\text{Mg}_x\text{Zn}_{1-x}\text{O}$ as a function of the composition x are shown. With increasing x , rock salt only shows a slight decrease (less than 1%) of both a and c , keeping the c/a ratio more or less constant (close to the ideal ratio for face centered cubic (FCC) hexagonal cells $\frac{2}{3}\frac{c}{a} = \frac{2}{3}\sqrt{6} \approx 1.633$). For ZB, both a and c increase, and also for this phase the ratio c/a remains close to ideal. The wurtzite phase on the other hand, displays an increase of a , and a decrease of c , which changes the c/a ratio from 1.61 (ZnO) to 1.54 (MgO).

The slabs used for the surface energy calculations

The slabs used for the surface energy calculations are shown in figures S4 and S5. Also shown in Fig. S5 is the cell used in calculating the RS (001) Mg-ZnO interface energy.

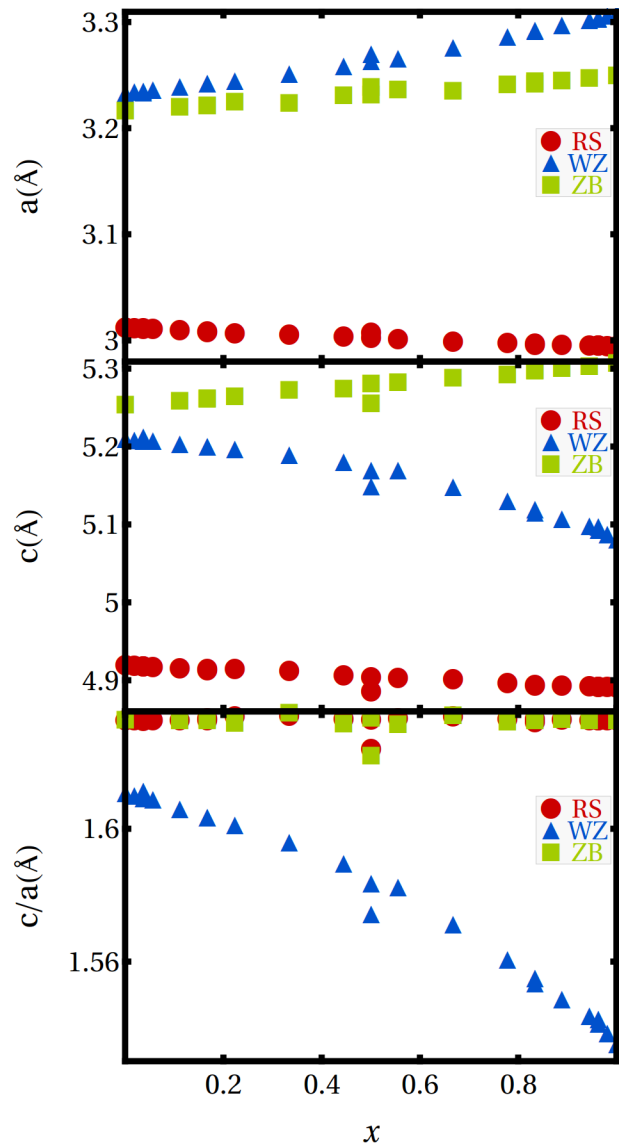


Figure S3: Lattice parameters a , c (a_{hex} and $\frac{2}{3}c_{\text{hex}}$ for bulk RS and bulk ZB phases, for comparison), and their ratio $\frac{c}{a}$ as a function of x .

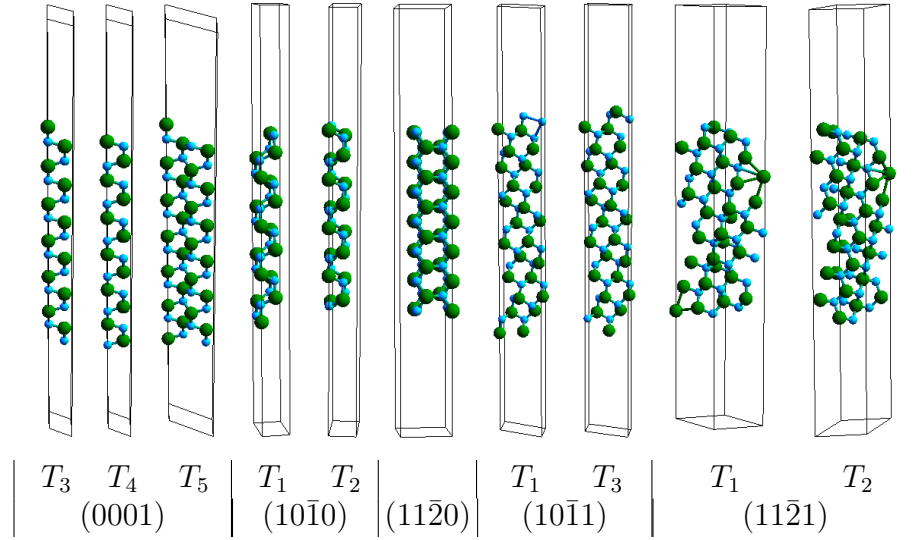


Figure S4: The wurtzite slabs used in the surface calculations. Different T's denote different terminations. Slabs T_i not shown are equivalent to T_{i-1} with Zn(Mg) and O -atoms interchanged.

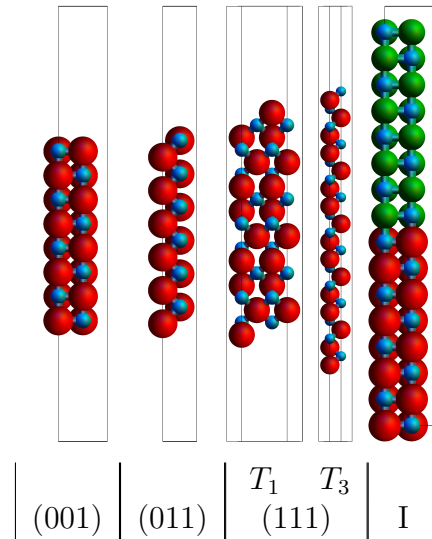


Figure S5: The rock salt slabs used in the surface calculations. Different T's denote different terminations. The cell labeled I is the rock salt (001) interface.

Hubbard U

Before applying the Hubbard U correction to the supercells, its effects on the ZnO unit cell must be studied. In order to find the optimum U parameter for ZnO, a scan over U -values was done for the wurzite unit cell. Lattice parameters, the position of the d -bands and the band-gap as a function of U are shown in Figures S6 and S7. Since the Hubbard U correction was introduced to push the d -bands down, a value of U should be chosen such that the position of the d -bands with respect to the valence band maximum (VBM) is in agreement with X-ray photoelectron spectroscopy (XPS) and ultraviolet photoelectron spectroscopy (UPS) experiments.⁸⁻¹⁶ The more recent measurements place the d -bands at 7.5 to 8.0 eV below the valence band maximum (VBM). Figure S7b shows that the DFT+ U calculations obtain the correct position of the d -bands when $U = 5.0$, and thus, this value was used for the Zn $3d$ electrons in all of the present calculations.

In figure S8 the dependence of the density of states on the parameter U can be seen. The d -bands move down with increasing U and the band gap widens.

In Figures S9 and S10 the densities of states of the wurzite and rock salt structures are plotted. The formation of the d -bands as x decreases can be clearly seen.

Bader Charge Distribution

In Figure S11 the Bader charges of the atoms of the slab as a function of the vertical coordinate are shown. The (unfavorable) $(0001)_{T_3}$ surface shows a considerable amount of charge redistribution: $-0.8e$ (compared to bulk) is transferred from the terminating oxygen atom to the terminating Zn atom. For the $(0001)_{T_4}$ surface a similar but smaller ($-0.2e$) effect is observed. This charge redistribution can reduce the dipole moment and therefore lower the energy of the surface. Of course, these results are for crystals in vacuum and strong surface tension and/or dielectric effects of a liquid phase may alter the results significantly.

In figures S12 through S17 the charges on the atoms of the various surface slabs are plotted as a function of the vertical coordinate z .

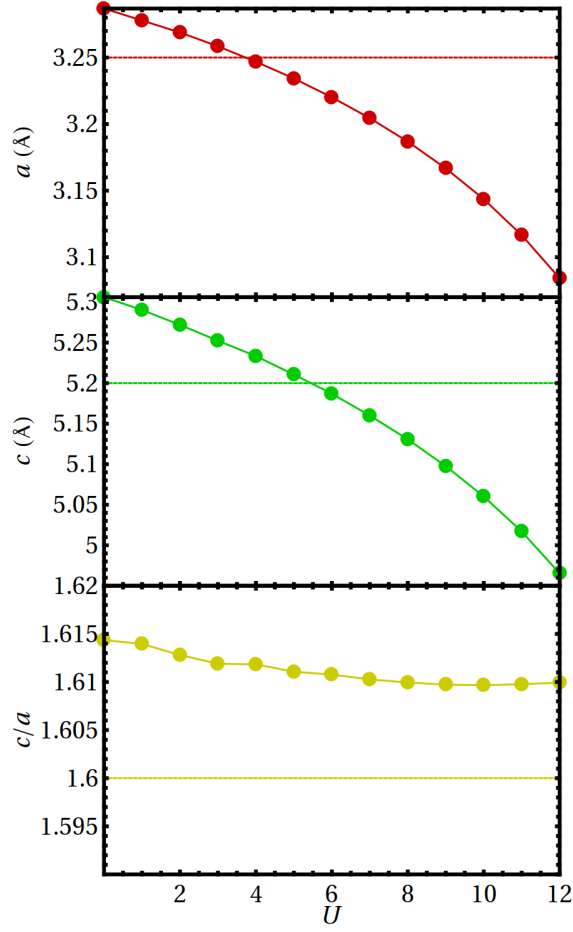


Figure S6: Lattice parameters a and c and their ratio as a function of the Hubbard U -value. Dashed horizontal lines indicate experimental values.

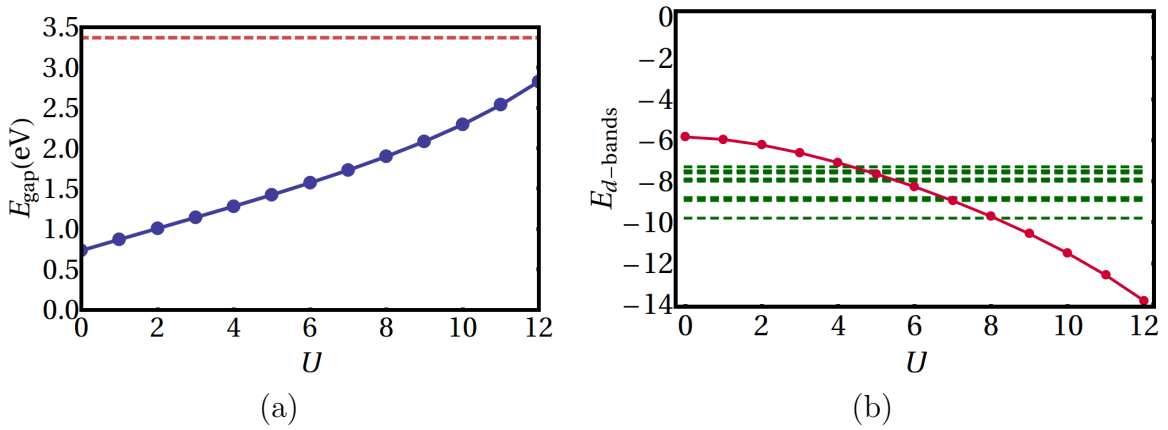


Figure S7: (a) Bandgap E_{gap} and (b) the position $E_{d\text{-bands}}$ of the d -bands relative to the valence band maximum as a function of the Hubbard U correction U . Horizontal lines are experimental values found in the literature.^{8–12,14–21}

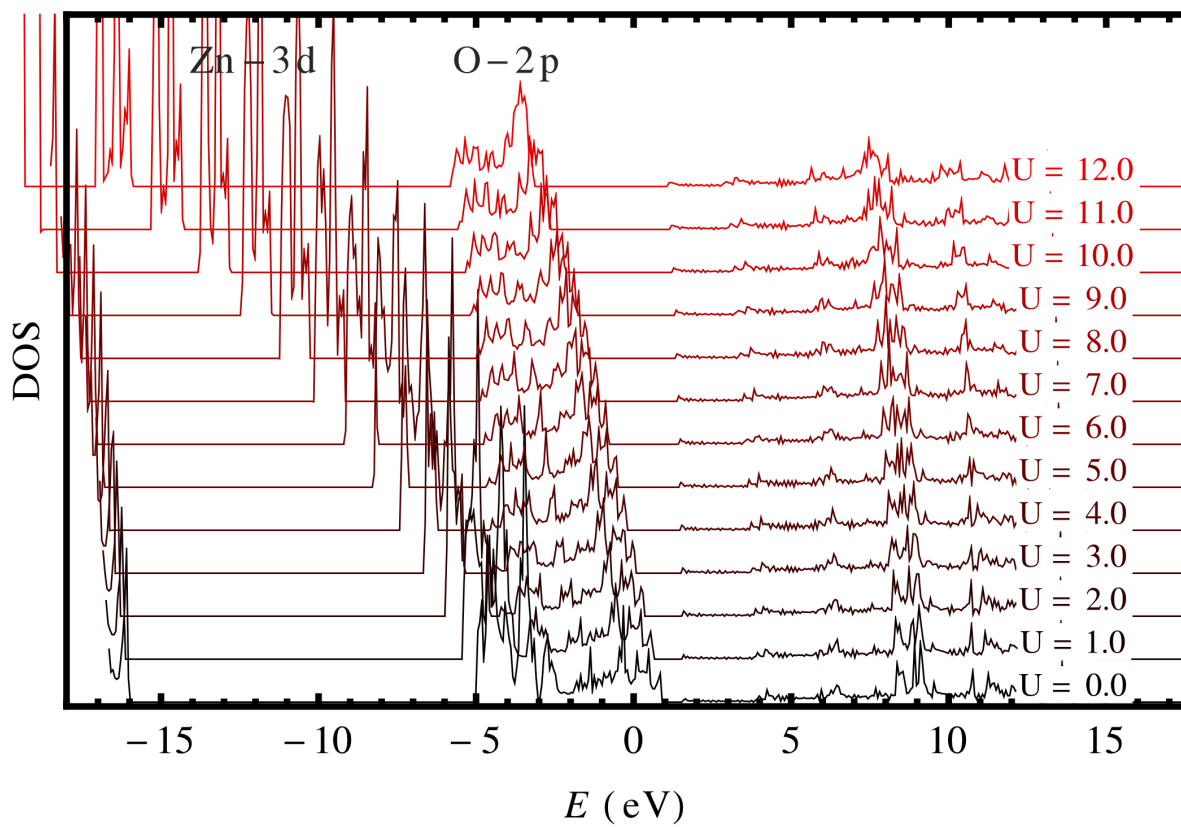


Figure S8: DOS plots for different values of U .

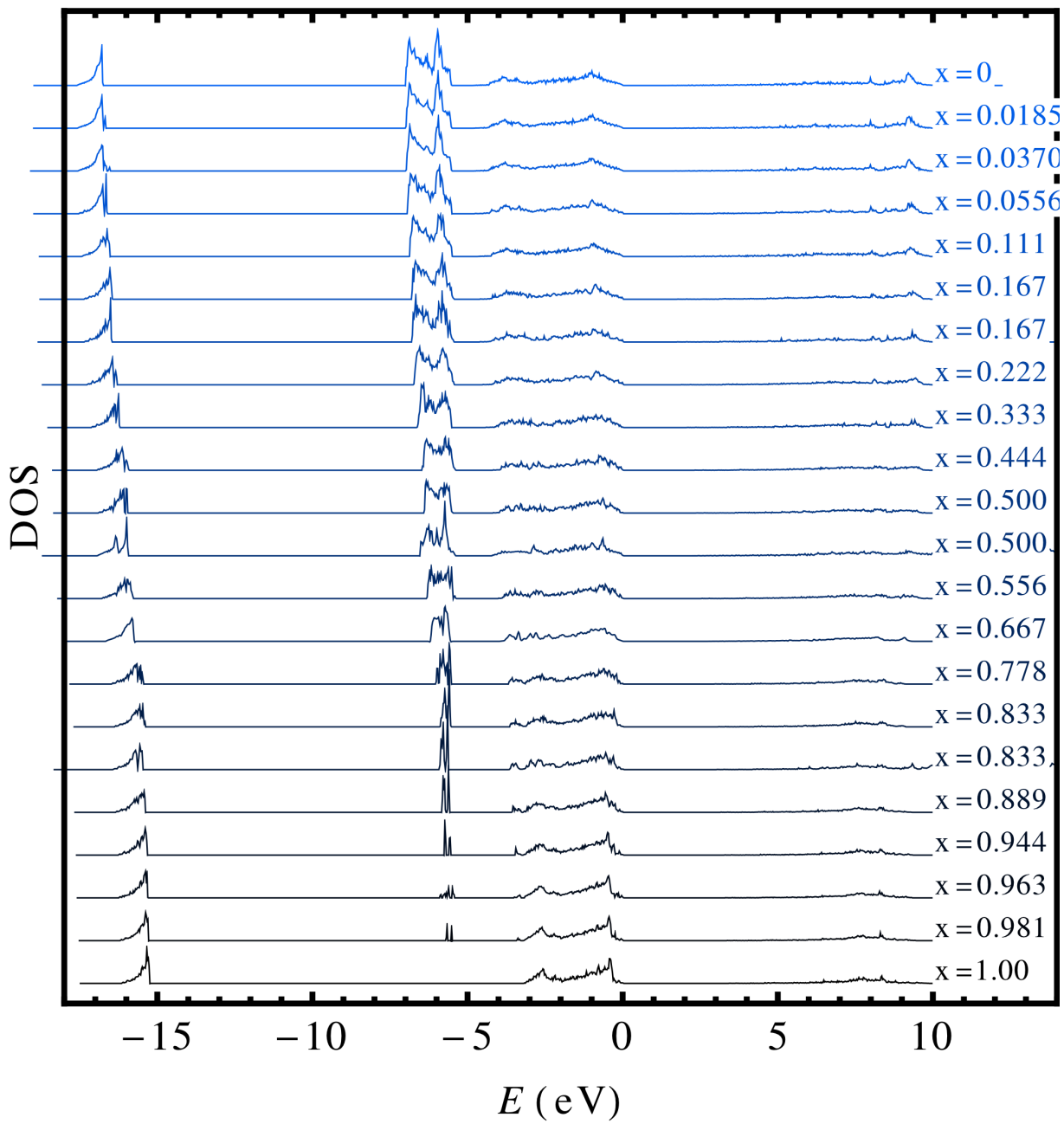


Figure S9: The density of states of wurtzite $\text{Mg}_x\text{Zn}_{1-x}\text{O}$ for several values of x .

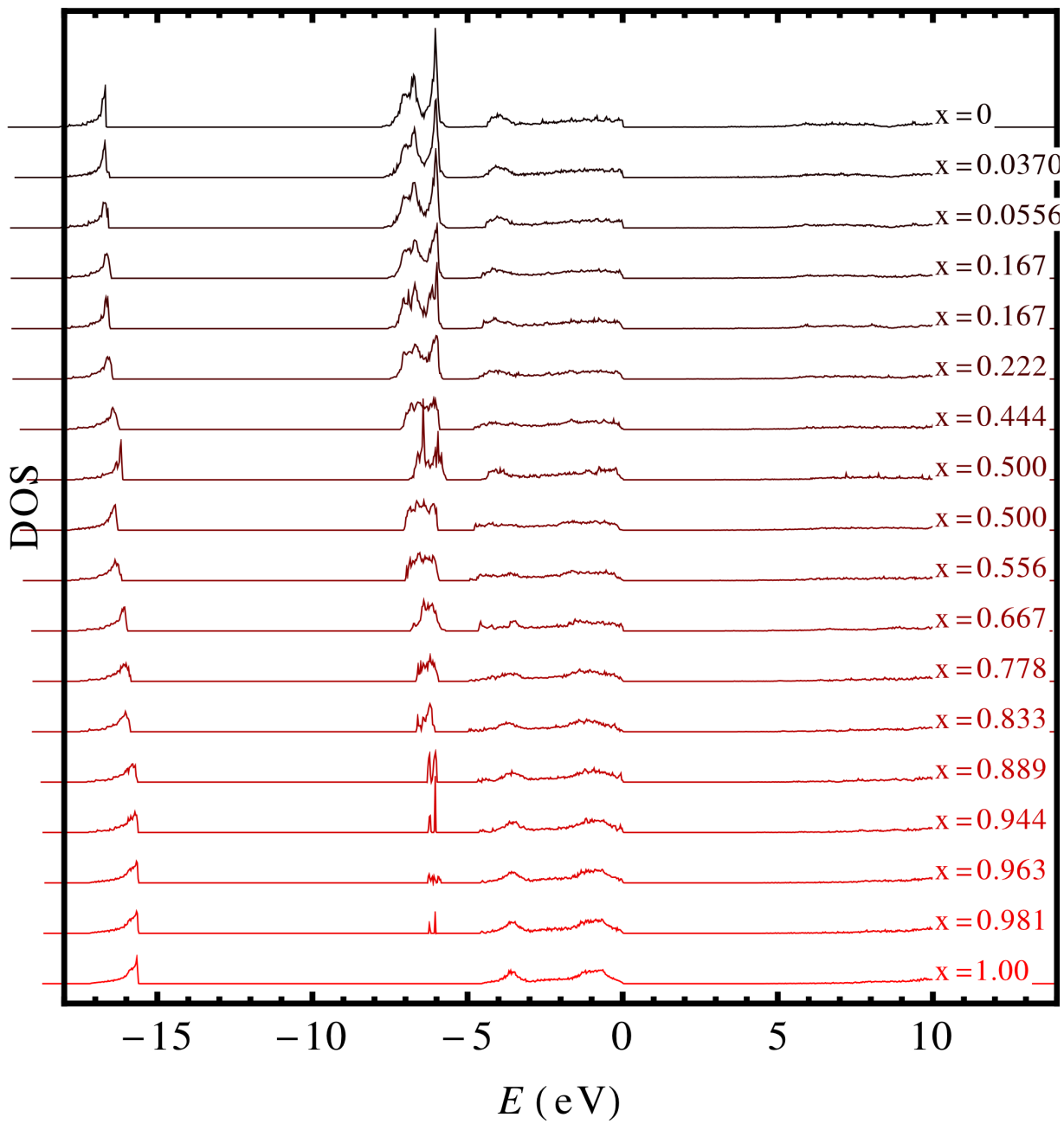


Figure S10: The density of states of rock salt $\text{Mg}_x\text{Zn}_{1-x}\text{O}$ for several values of x .

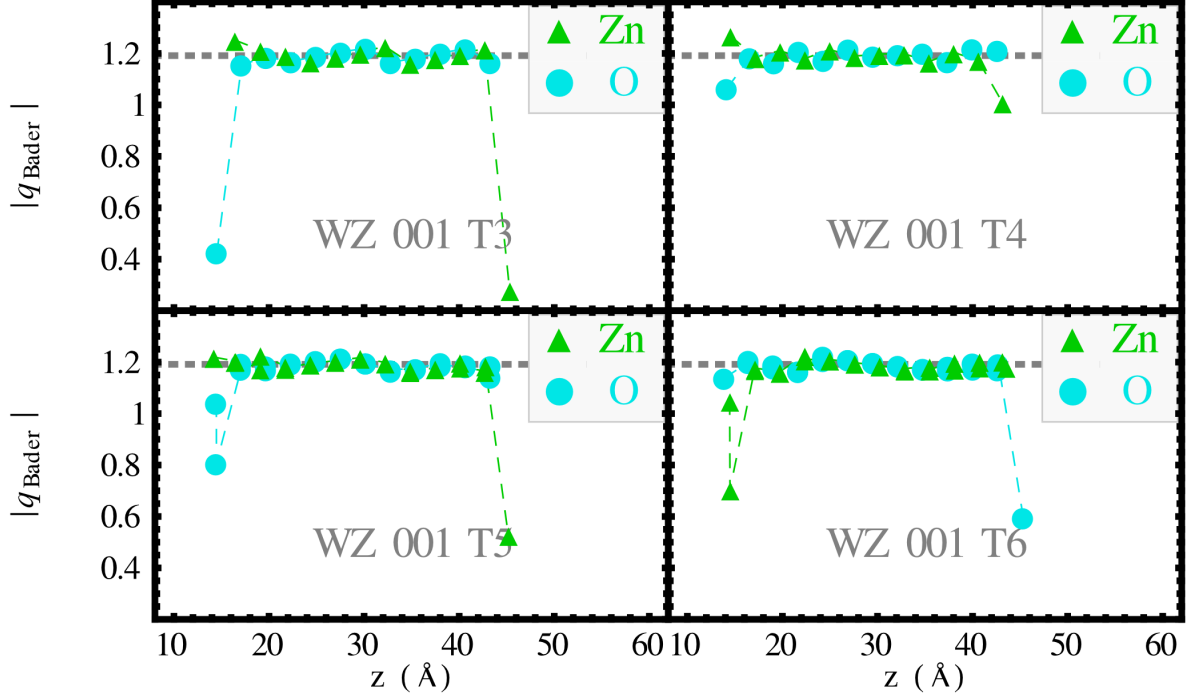


Figure S11: Absolute value of the Bader charge of the atoms in the wurtzite (000 $\bar{1}$) slabs as a function of the vertical coordinate of the atoms.

Total energies of the particles

To obtain the phase diagram shown in Fig. 10 in the main text, the following expressions were used: For the ZnO terminated $\text{Mg}_x\text{Zn}_{1-x}\text{O}$ mixed phases, the total energy per formula unit as a function of composition x , size N (number of formula units) and temperature T is given by:

$$E_{\text{B+S}}^\phi(x, N, T) = E_B^\phi(x) - T s_{\text{conf}}(x) + \frac{\min(1, \xi) E_{S, \text{ZnO}}^\phi + \max(0, 1 - \xi) E_{S, \text{MgO}}^\phi}{N^{\frac{1}{3}}}, \quad (1)$$

where $\phi = \text{RS}, \text{WZ}, \text{ZB}$, $E_B^\phi(x)$ is the bulk energy per formula unit, $s(x)$ is the configurational entropy per formula unit. The correction factor x is introduced to account for the possibility that there may not be enough Zn in the particle to cover the surface, and $E_{S,i}^\phi$ (with $i =$

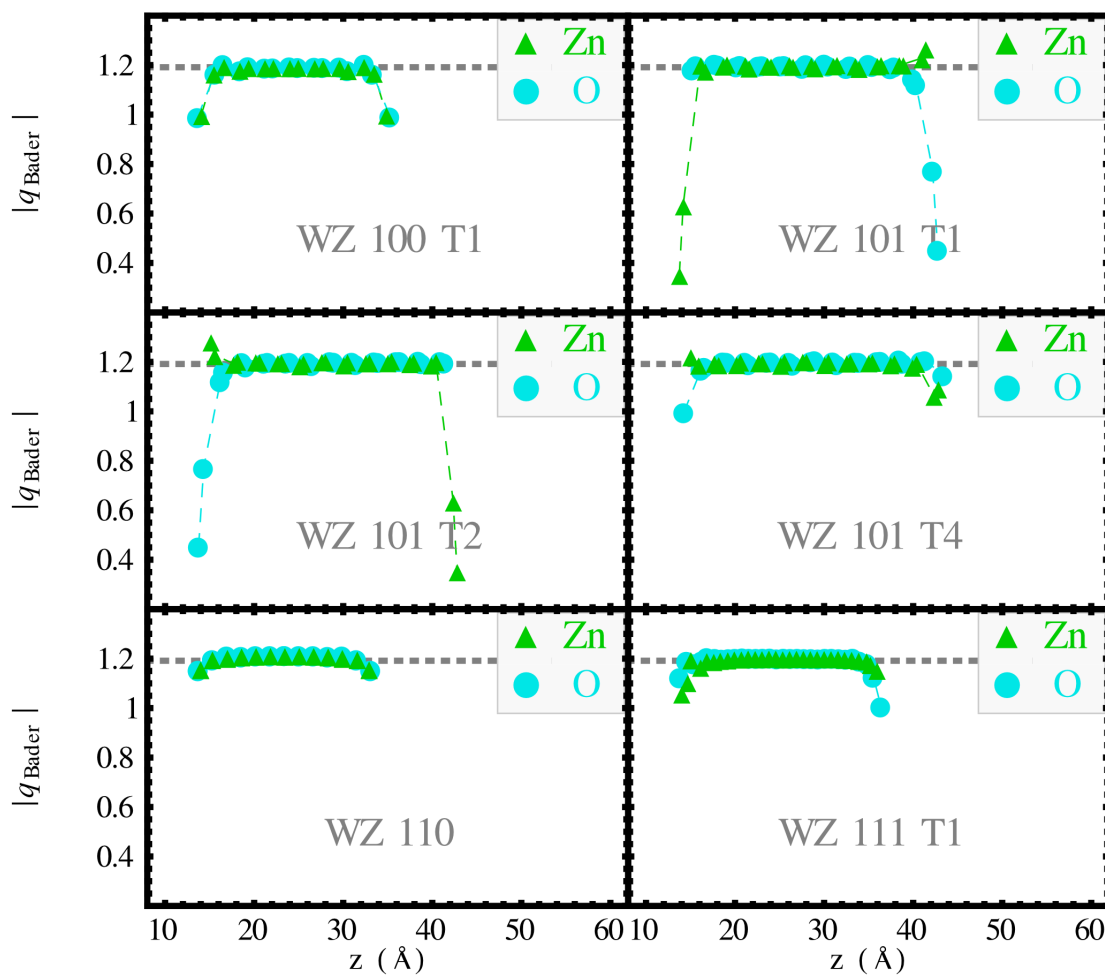


Figure S12: Absolute value of the Bader charge of the atoms of the wurzite ZnO slabs as a function of the vertical coordinate of the atoms.

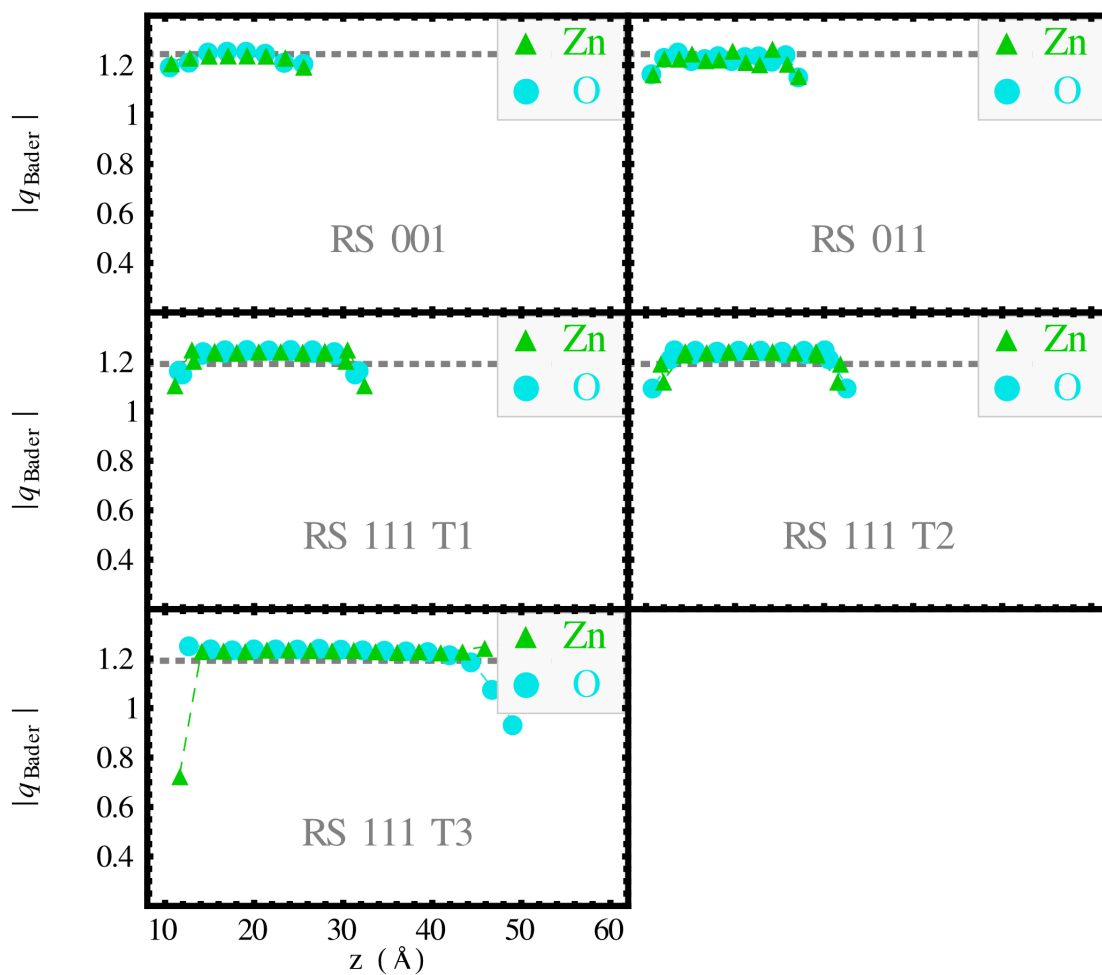


Figure S13: Absolute value of the Bader charge of the atoms of the rock salt ZnO slabs as a function of the vertical coordinate of the atoms.

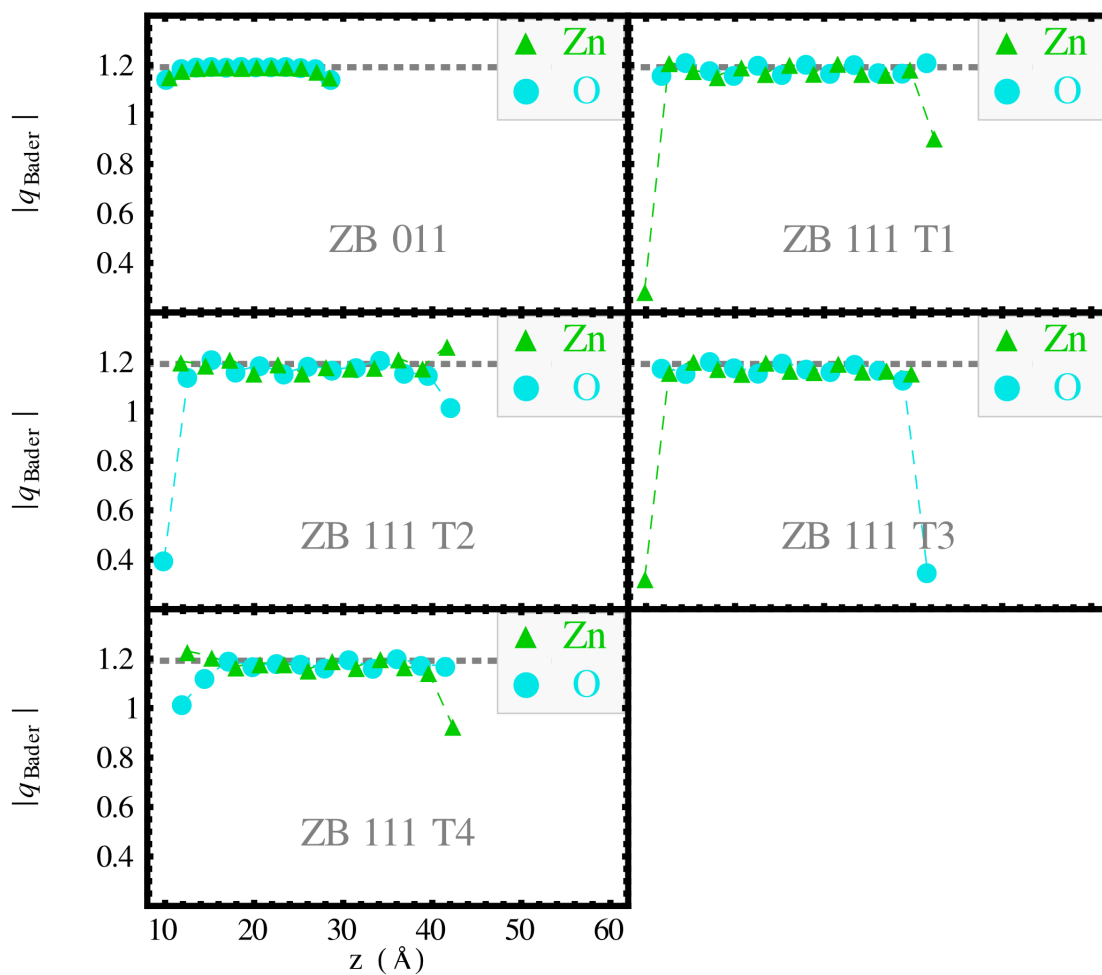


Figure S14: Absolute value of the Bader charge of the atoms of the zinc blend ZnO slabs as a function of the vertical coordinate of the atoms.

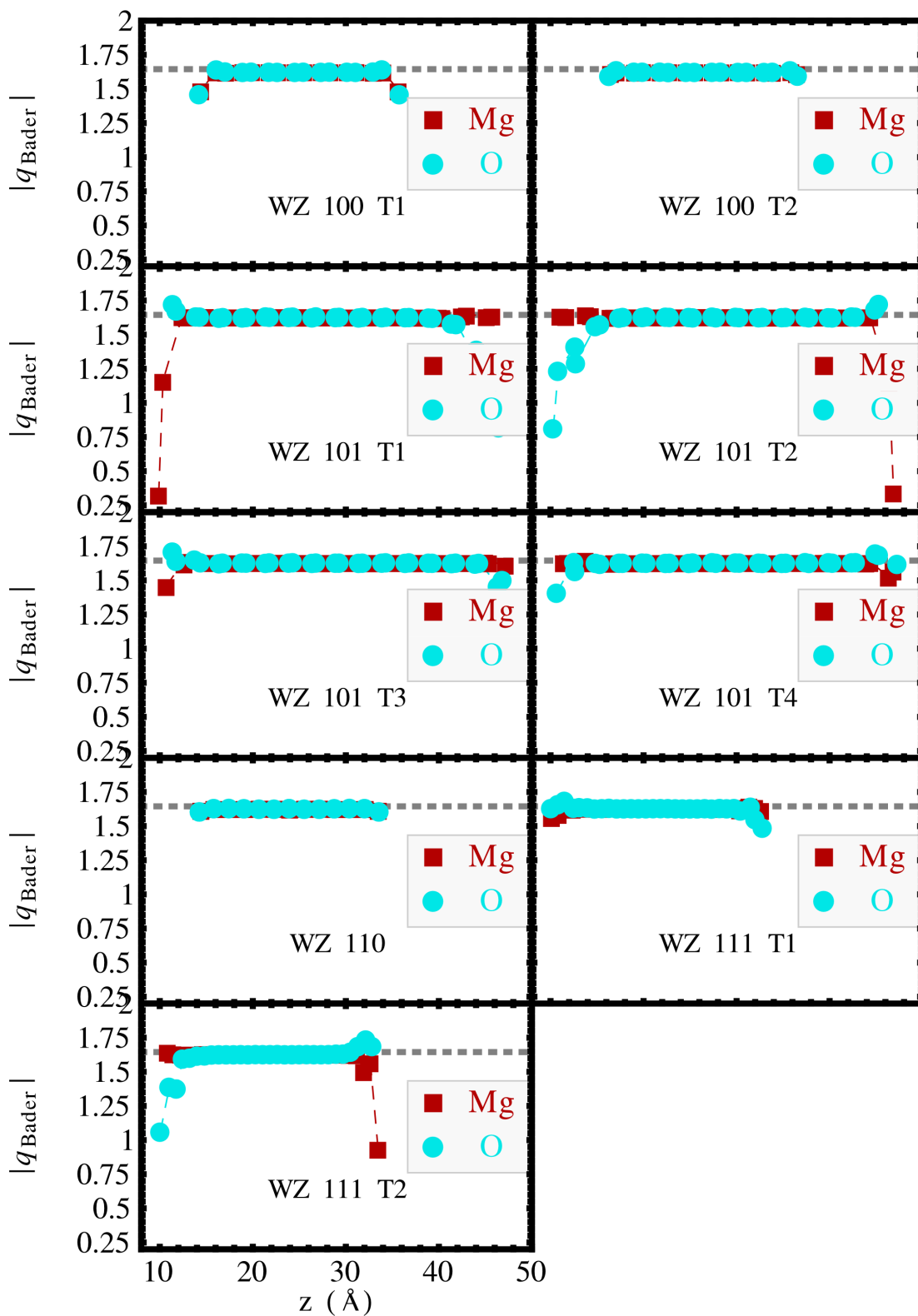


Figure S15: Absolute value of the Bader charge of the atoms of the wurzite MgO slabs as a function of the vertical coordinate of the atoms.

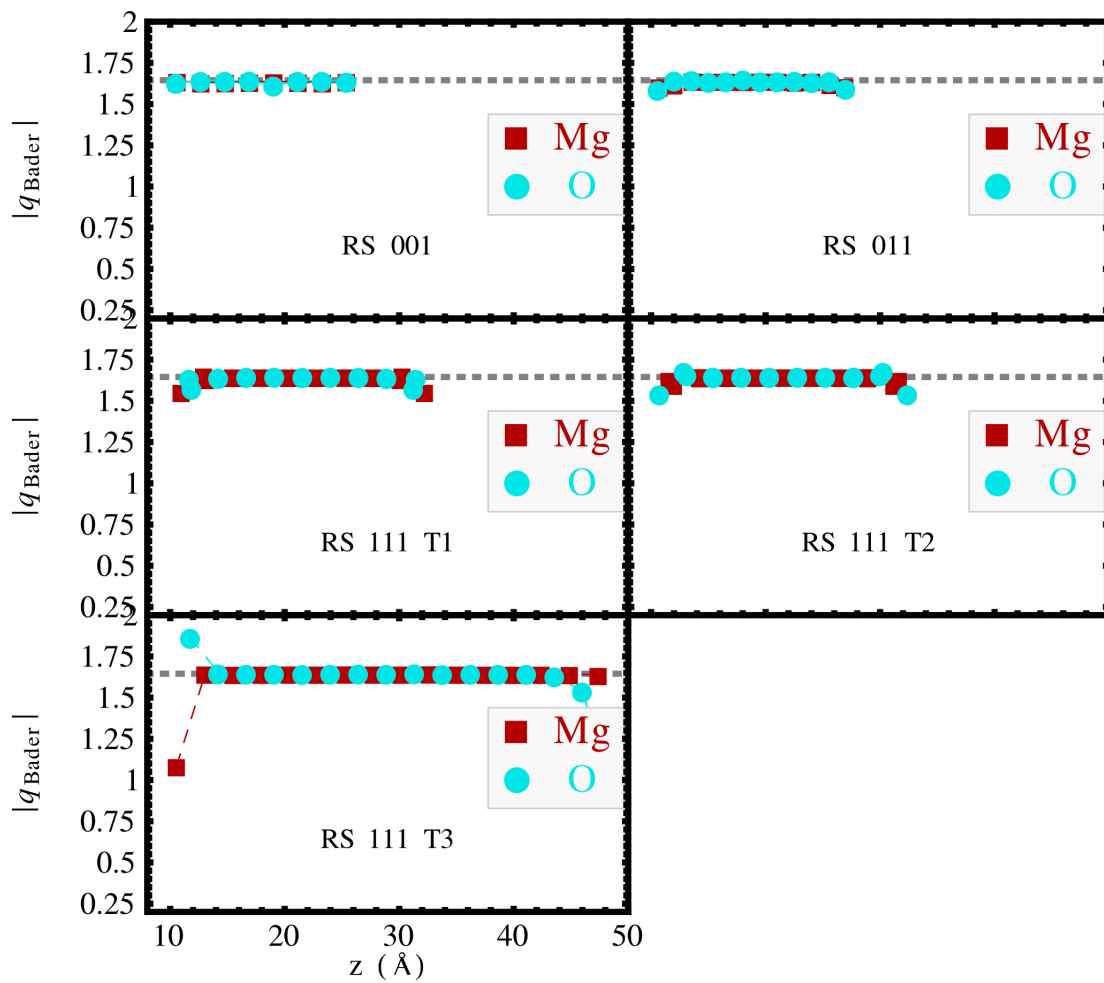


Figure S16: Absolute value of the Bader charge of the atoms of the rock salt MgO slabs as a function of the vertical coordinate of the atoms.

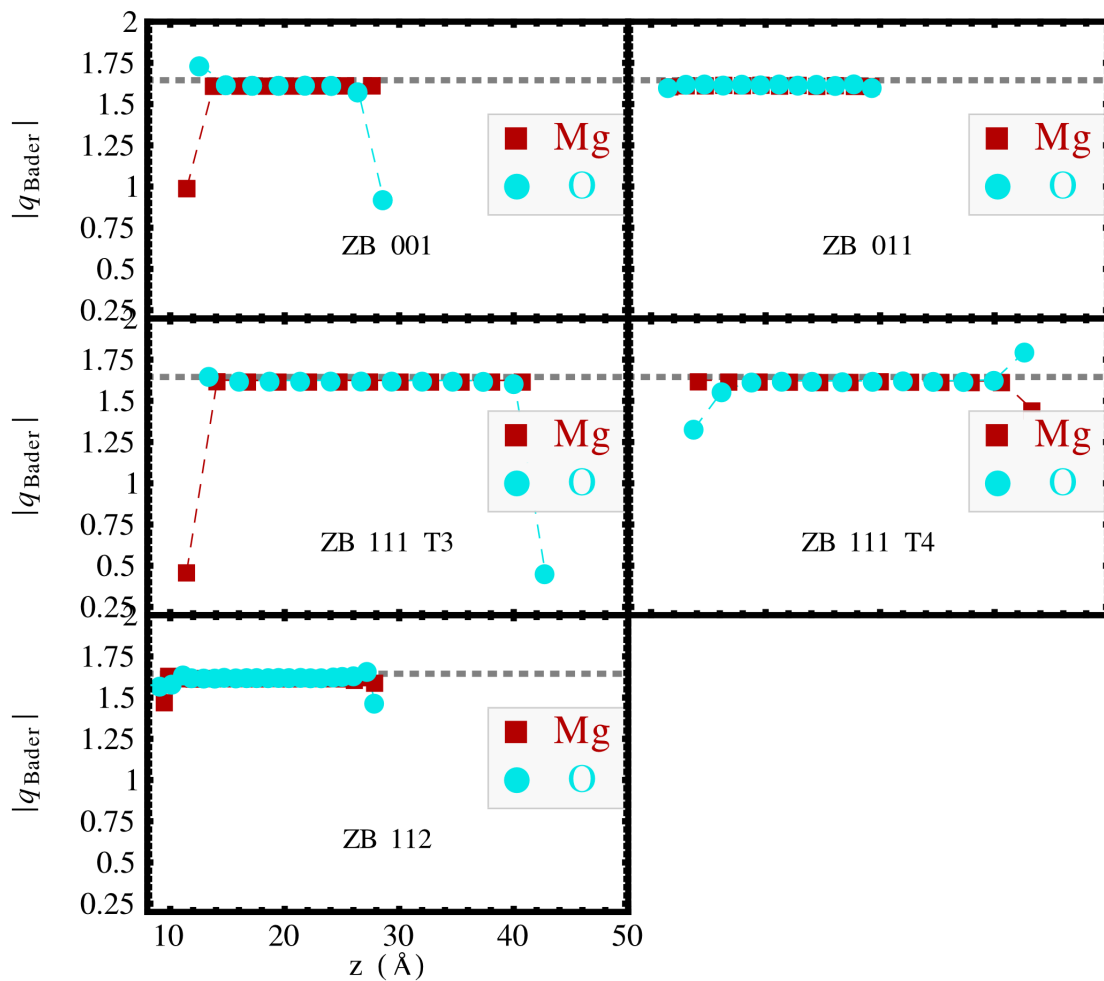


Figure S17: Absolute value of the Bader charge of the atoms of the zinc blend MgO slabs as a function of the vertical coordinate of the atoms.

MgO, ZnO) is the rescaled surface energy:

$$\xi = \frac{(1-x)N}{(xc_{\text{MgO}}^\phi + (1-x)c_{\text{ZnO}}^\phi)(N^{\frac{1}{3}} - 1)^2}, \quad (2)$$

$$E_{S,i}^\phi = \frac{\sum_j^{\text{surfaces}} \gamma_{i,j}^\phi A_j}{\sum_j^{\text{surfaces}} A_j} c_i^\phi, \quad (3)$$

where $\gamma_{i,j}^\phi$ is the (lowest) surface energy of a surface j , and A_j the the surface area of that particular surface, and $c_i^\phi = A_{\text{tot}}/V_{\text{tot}}^{2/3}$ is a morphology dependent constant ($c = 6$ for cubes (RS), $c = 6 \cdot 2^{-\frac{1}{6}} \approx 5.345$ for rhombic dodecahedra (ZB), and $c_{\text{MgO}}^{\text{WZ}} \approx 5.417$, $c_{\text{ZnO}}^{\text{WZ}} \approx 5.783$).

According to the bulk calculations the $\text{Mg}_x\text{Zn}_{1-x}\text{O}$ mixed phases are only stable when x is near 0 or 1, otherwise the system will phase separate. We therefore also compare with the energy of a system of phase separated particles of size N :

$$E^{\text{Ph.Sep.}}(x, N, T) = \begin{cases} E_B^{\text{WZ}}(x) - T s_{\text{conf}}(x) + \frac{x E_{S,\text{MgO}}^{\text{WZ}} + (1-x) E_{S,\text{ZnO}}^{\text{WZ}}}{N^{\frac{1}{3}}} & x < x_{\text{max}}^{\text{WZ}} \\ y \left[E_B^{\text{RS}}(x_{\text{min}}^{\text{RS}}) - T s_{\text{conf}}(x_{\text{min}}^{\text{RS}}) + \frac{x_{\text{min}}^{\text{RS}} E_{S,\text{MgO}}^{\text{RS}} + (1-x_{\text{min}}^{\text{RS}}) E_{S,\text{ZnO}}^{\text{RS}}}{N^{\frac{1}{3}}} \right] + \\ (1-y) \left[E_B^{\text{WZ}}(x_{\text{max}}^{\text{WZ}}) - T s_{\text{conf}}(x_{\text{max}}^{\text{WZ}}) + \frac{x_{\text{max}}^{\text{WZ}} E_{S,\text{MgO}}^{\text{WZ}} + (1-x_{\text{max}}^{\text{WZ}}) E_{S,\text{ZnO}}^{\text{WZ}}}{N^{\frac{1}{3}}} \right] & x_{\text{max}}^{\text{WZ}} < x < x_{\text{min}}^{\text{RS}} \\ E_B^{\text{RS}}(x) - T s_{\text{conf}}(x) + \frac{x E_{S,\text{MgO}}^{\text{RS}} + (1-x) E_{S,\text{ZnO}}^{\text{RS}}}{N^{\frac{1}{3}}} & x_{\text{min}}^{\text{RS}} < x \end{cases}, \quad (4)$$

where $x_{\text{max}}^{\text{WZ}}(T)$ and $x_{\text{min}}^{\text{RS}}(T)$ are the maximal value for which bulk WZ $\text{Mg}_x\text{Zn}_{1-x}\text{O}$ is stable and the minimal value for which bulk RS $\text{Mg}_x\text{Zn}_{1-x}\text{O}$ is stable, respectively, i.e. the boundaries in Fig. 3 in the main text. The fraction of RS particles $y = (x - x_{\text{max}}^{\text{WZ}})/(x_{\text{min}}^{\text{RS}} - x_{\text{max}}^{\text{WZ}})$ is such that the total fraction of Mg atoms is x .

The last configuration we consider is a core-shell particle, with a MgO-rich core, a ZnO-rich shell and a fully ZnO terminated surface, if possible. We will assume that the compositions of core and shell are $x_{\text{min}}^{\text{RS}}$ and $x_{\text{max}}^{\text{WZ}}$ respectively, even though here both phases are rock

salt. We have used the following formula:

$$E^{\text{CS}}(x, N, T) = \begin{cases} y \left[E_B^{\text{RS}}(x_{\min}^{\text{RS}}) - T s_{\text{conf}}(x_{\min}^{\text{RS}}) \right] + \\ \quad + (1 - y) \left[E_B^{\text{WZ}}(x_{\max}^{\text{WZ}}) - T s_{\text{conf}}(x_{\max}^{\text{WZ}}) \right] + \\ \quad + \frac{\min(1, \xi) E_{S, \text{ZnO}}^{\text{RS}} + \max(0, 1 - \xi) E_{S, \text{MgO}}^{\text{RS}}}{N^{\frac{1}{3}}} \\ \quad + \frac{E_{\text{interface}} \max(0, y)^{\frac{2}{3}}}{N^{\frac{1}{3}}} & x_{\max}^{\text{WZ}} < x < x_{\min}^{\text{RS}}, \\ E_B^{\text{RS}}(x) - T s_{\text{conf}}(x) + \frac{\min(1, \xi) E_{S, \text{ZnO}}^{\text{RS}} + \max(0, 1 - \xi) E_{S, \text{MgO}}^{\text{RS}}}{N^{\frac{1}{3}}} & \text{otherwise} \end{cases}, \quad (5)$$

where $E_{\text{interface}} = \gamma_{\text{interface}} A_{\text{core}}$ with $\gamma_{\text{interface}}$ interface energy obtained in the calculation of the RS (100) MgO - RS (100) ZnO interface described in the main text, and A_{core} the surface area of the core.

References

1. Kresse, G.; Furthmüller, J. Efficiency of Ab-Initio Total Energy Calculations for Metals and Semiconductors Using a Plane-Wave Basis Set. *Computational Materials Science* **1996**, *6*, 15–50.
2. Hohenberg, P.; Kohn, W. Inhomogeneous Electron Gas. *Physical Review* **1964**, *136*, B864–B871.
3. Kohn, W.; Sham, L. J. Self-Consistent Equations Including Exchange and Correlation Effects. *Physical Review* **1965**, *140*, A1133–A1138.
4. Kohn, W. Nobel Lecture: Electronic Structure of Matter - Wave Functions and Density Functional. *Reviews of Modern Physics* **1999**, *71*, 1253–1266.
5. Perdew, J. P.; Burke, K.; Ernzerhof, M. Generalized Gradient Approximation Made Simple. *Physical Review Letters* **1996**, *77*, 3865–3868.
6. Kresse, G.; Joubert, D. From Ultrasoft Pseudopotentials to the Projector Augmented-

- Wave Method. *Physical Review B - Condensed Matter and Materials Physics* **1999**, *59*, 1758–1775.
7. Blöchl, P. E. Projector Augmented-Wave Method. *Physical Review B* **1994**, *50*, 17953–17979.
 8. Ley, L.; Pollak, R. A.; McFeely, F. R.; Kowalczyk, S. P.; Shirley, D. A. Total Valence-Band Densities of States of III-V and II-VI Compounds from X-Ray Photoemission Spectroscopy. *Physical Review B* **1974**, *9*, 600–621.
 9. Zwicker, G.; Jacobi, K. Site-specific interaction of H₂O with ZnO single-crystal surfaces studied by thermal desorption and UV photoelectron spectroscopy. *Surface Science* **1983**, *131*, 179–194.
 10. Ye, Z. Z.; Zeng, Y. J.; Lu, Y. F.; Lin, S. S.; Sun, L.; Zhu, L. P.; Zhao, B. H. Donor/acceptor doping and electrical tailoring in ZnO quantum dots. *Applied Physics Letters* **2007**, *91*.
 11. Zeng, Y. J.; Ye, Z. Z.; Liu, F.; Li, D. Y.; Lu, Y. F.; Jaeger, W.; He, H. P.; Zhu, L. P.; Huang, J. Y.; Zhao, B. H. Controllable growth and characterization of ZnO/MgO quasi core-shell quantum dots. *Crystal Growth and Design* **2009**, *9*, 263–266.
 12. Sharma, B. K.; Khare, N.; Kumar, M. Stress dependent band gap shift and valence band studies in ZnO nanorods. *Journal of Nanoscience and Nanotechnology* **2010**, *10*, 8424–8431.
 13. White, M. A.; Lovejoy, T. C.; Ochsenein, S. T.; Olmstead, M. A.; Gamelin, D. R. Sputtering-induced CoO formation in x-ray photoelectron spectroscopy of nanocrystalline Zn_{1-x}Co_xO spinodal enrichment models. *Journal of Applied Physics* **2010**, *107*.
 14. Blumentrit, P.; Yoshitake, M.; Nemk, S.; Kim, T.; Nagata, T. XPS and UPS study on

- band alignment at Pt-Zn-terminated ZnO(0 0 0 1) interface. *Applied Surface Science* **2011**, *258*, 780–785.
15. Guo, P.; Jiang, J.; Shen, S.; Guo, L. ZnS/ZnO heterojunction as photoelectrode: Type II band alignment towards enhanced photoelectrochemical performance. *International Journal of Hydrogen Energy* **2013**, Article in Press.
 16. Yan, X.; Itoh, T.; Dai, S.; Ozaki, Y.; Fang, Y. Cu, Mn doping effect to optical behavior and electronic structure of ZnO ceramic. *Journal of Physics and Chemistry of Solids* **2013**, *74*, 1127–1130.
 17. Strunskus, T.; Fuchs, O.; Weinhardt, L.; Heske, C.; Guraya, M.; Muhler, M.; Staemmler, V.; Wll, C. The valence electronic structure of zinc oxide powders as determined by X-ray emission spectroscopy: variation of electronic structure with particle size. *Journal of Electron Spectroscopy and Related Phenomena* **2004**, *134*, 183 – 189.
 18. Lin, Y. .; Chang, S. .; Chang, H. .; Liu, Y. . High-barrier rectifying contacts on undoped ZnO films with (NH₄)₂Sx treatment owing to Fermi-level pinning. *Journal of Physics D: Applied Physics* **2009**, *42*.
 19. Sahu, R. K.; Ganguly, K.; Mishra, T.; Mishra, M.; Ningthoujam, R. S.; Roy, S. K.; Pathak, L. C. Stabilization of intrinsic defects at high temperatures in ZnO nanoparticles by Ag modification. *Journal of colloid and interface science* **2012**, *366*, 8–15.
 20. Cong, G. W.; Peng, W. Q.; Wei, H. Y.; Han, X. X.; Wu, J. J.; Liu, X. L.; Zhu, Q. S.; Wang, Z. G.; Lu, J. G.; Ye, Z. Z. *et al.* Comparison of valence band x-ray photoelectron spectrum between Al-N-codoped and N-doped ZnO films. *Applied Physics Letters* **2006**, *88*.
 21. Perkins, C. L.; Lee, S. .; Li, X.; Asher, S. E.; Coutts, T. J. Identification of Nitrogen Chemical States in N-doped ZnO via X-ray Photoelectron Spectroscopy. *Journal of Applied Physics* **2005**, *97*.